EARTHQUAKE ENGINEERING AND STRUCTURAL DYNAMICS
Earthquake Engng. Struct. Dyn. **27**, 1445–1464 (1998)

SEISMIC RESPONSE OF STEEL FRAME BUILDINGS TO NEAR-SOURCE GROUND MOTIONS

JOHN F. HALL*,†
Division of Engineering and Applied Science, Caltech, Pasadena, CA 91125, U.S.A.

SUMMARY

Simulated ground motions from the M_W 6·7 Northridge earthquake and a simulated M_W 7·0 Elysian Park event are generated over a large grid of sites and used as input to mathematical models of six-storey and 20-storey steel-frame buildings. Purpose of the study is to quantify effects of strong near-source ground motion on frame buildings of different height and strength (UBC vs. Japanese design) and with welded connections prone to fracture. Best performance is achieved by the six-storey building which meets the stronger Japanese design provisions. The detrimental effect of connection fracture is significant, especially for the larger earthquake. © 1998 John Wiley & Sons, Ltd.

KEY WORDS: earthquake engineering; near-source effects; Northridge earthquake; steel buildings; weld fracture

1. INTRODUCTION

Strong near-source ground motions contain large, rapid displacement pulses which can have severe effects on structures. Of interest are ground displacements exceeding half a meter which take place at ground velocities on the order of a meter per second. In the U.S. it is generally agreed that our previous design codes do not adequately address this kind of ground motion, and changes are being made to increase the design force levels, which will result in stronger and stiffer buildings. In Japan, the design force levels for buildings have for some time been considerably greater than in the U.S. Even so, Japanese engineers are also concerned about the adequacy of their design provisions for strong near-source effects.

The issue of building strength appropriate for near-source ground motions is investigated in this report. Two different heights of buildings are selected, 6 storyes and 20 storyes, and for each height, designs of two different strengths are produced. The first design is according to the 1994 Uniform Building Code,[1] and the second design follows Japanese provisions.[2] All four buildings are steel moment frames. The UBC designs are intended to be typical of existing structures in Zone 4 in the U.S.

One important part of assessing near-source ground motions is to quantify the size of the region which is affected. An aspect of this is that near-source effects are most pronounced over only a portion of the near-fault zone, the region toward which the fault is rupturing. In this study, ground motions at a grid of sites sufficient to cover the region of near-source effects are employed. This is accomplished by using simulated ground motions. Two earthquakes are considered here: 1994 Northridge (M_W 6·7) and a hypothetical M_W 7·0 event on the Elysian Park fault in Los Angeles.

Previous studies of strong near-source ground motions have shown the potential for large storey drifts in buildings and even collapse.[3–8] Future design measures may have to consider all contributions to the

* Correspondence to: John F. Hall, Division of Engineering and Applied Science, Mail Code 104-44, Caltech, Pasadena, CA 91125, U.S.A. E-mail: johnhall@cco.caltech.edu
† Professor of Civil Engineering

Contract/grant sponsor: Kajima-CUREe Joint Research Program

CCC 0098–8847/98/121445–20$17·50

Received 2 October 1997
Revised 17 March 1998

strength of a building in order to be feasible. It follows from this that since future design methods will be based on assessment studies like the present one, the assessments should also be done as realistically as possible and include all important contributions to the strength of a structure. Such an approach is followed here. In addition, since strong near-source ground motions will likely produce severely non-linear responses, it becomes necessary to include structural degradation effects. In this study, due to the common occurrence of welded-connection failure in the Northridge and Kobe earthquakes and because this behaviour seems to be an important degradation mode, treatment of connection fracture is included. As there is now wide-spread interest in fracture of welded connections,[8] this is an important part of the present investigation.

There is no particular reason for choosing steel buildings as opposed to reinforced concrete buildings as the object of this study. With the exception of the detrimental effects of weld fracture, the results presented here are probably also applicable to reinforced-concrete moment-frame buildings of similar strength and stiffness.

2. DESCRIPTIONS OF BUILDINGS

2.1. Design

A total of four steel moment-frame buildings are studied. They are referred to by the following notation: U6, a 6-storey-plus-basement building designed according to the 1994 Uniform Building Code; J6, a 6-storey-plus-basement building designed according to Japanese provisions; U20, a 20-storey-plus-basement building designed according to the 1994 Uniform Building Code; and J20, a 20-storey-plus-basement building designed according to Japanese provisions. Geometries of the buildings are shown in Figure 1. Floor plans, storey heights, and overall building dimensions are the same for U6 and J6, as are those for U20 and J20. All structural details are given in Reference 9. Only the earthquake response in the plane of the narrow dimension of the building is of interest here.

A36 steel is used for both beams and columns. Design dead loads are 3·83 kPa (80 psf) for the roof, 4·55 kPa (95 psf) for the floors, and 1·68 kPa (35 psf) for the cladding. The floor design live load is 2·39 kPa (50 psf).

Designs are carried out for gravity plus wind and gravity plus seismic loads. The design for the lateral loads does not include Frames B in U6, J6, U20 and J20 which contain only simply supported beams. Half-building models are used: a single Frame A for U6 and U20 and a single Frame A plus a half Frame C for J6 and J20. Panel zones of the columns are thickened, if necessary, to make the panel zone yield moment equal to 0·8 times the sum of the plastic moment capacities of the connecting beams; see the UBC.

Gravity loads are applied directly to the columns of the included frames based on tributary areas to these columns. Girders are not loaded within their spans. This treatment is consistent with intermediate floor beams running parallel to the short direction of the building. Gravity loads are computed using full dead load and a reduced 0·72 kPa (15 psf) of floor live load.

Horizontal seismic loads for U6 and U20 are based on the dead weight above ground level. The weight used to compute the horizontal seismic loads for J6 and J20 also includes 0·48 kPa (10 psf) of floor live load. The total above-ground (half) building weight used in the seismic design is denoted as W; values are listed below.

	U6	J6	U20	J20
W (MN)	12·80	13·76	31·30	33·83

UBC[1] design parameters for U6 and U20, including the resulting base shear coefficient V/W, are as follows:

	Z	I	R_W	S	T	C	V/W	drift limit
U6	0·4	1	12	1·2	1·22 sec	1·312	0·0437	0·25 %
U20	0·4	1	12	1·2	2·91 sec	0·736	0·0300	0·25 %

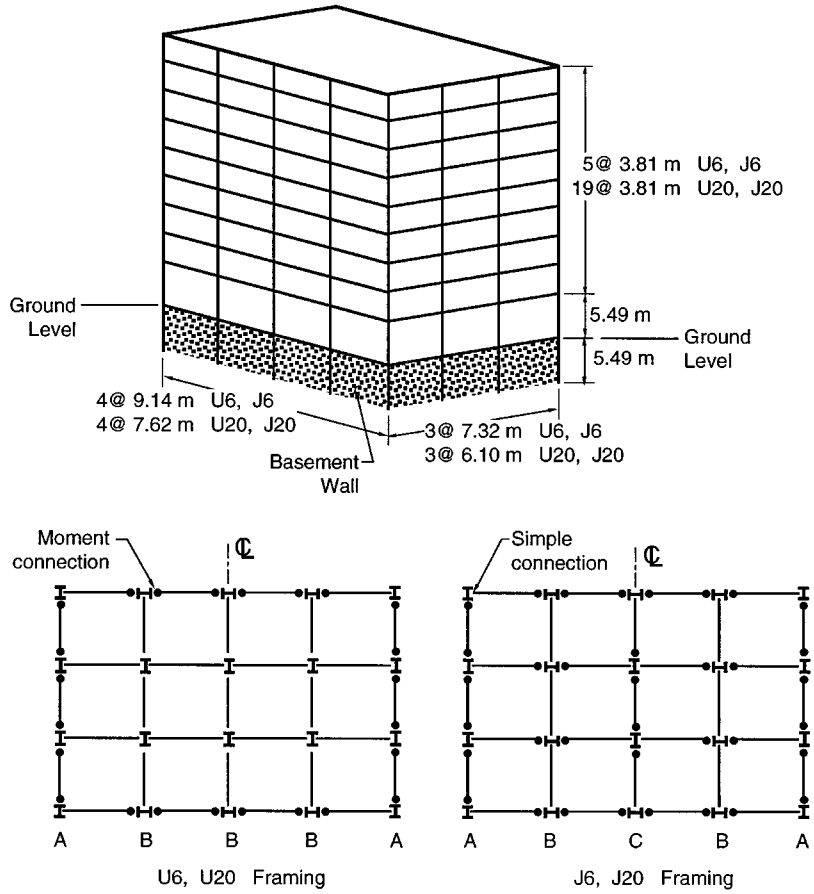

Figure 1. Geometries of the four buildings studied

Design parameters from the Japanese provisions[2] for J6 and J20, including the resulting base shear coefficient Q/W, are as follows:

	Z	Soil	T	R_t	C_o	Q/W	drift limit
J6	1	Type 2	0·73 sec	0·990	0·2	0·1980	—
J20	1	Type 2	2·34 sec	0·410	0·2	0·0820	0·50 %

The above base shear coefficients are for allowable stress design, and the nominal allowable stress for combined gravity and seismic is 90 per cent of the yield stress for the Japanese provisions and is computed using the 33 per cent increase for the UBC. The Japanese code also requires a check on ultimate strength. For J6 and J20, which are regular and symmetric buildings, the required ultimate strength corresponds to 1·25 of the base shear coefficient Q/W given above.

The period T for the UBC designs is taken as the code value $0{\cdot}035 \cdot (h_n)^{0{\cdot}75}$ plus the allowed increase of 30 per cent. In the drift calculation, the full design loads (without the reduction permitted by Section 1628.8.3 of the 1994 UBC) are applied, but with no eccentricity. This represents a net conservatism, especially for the 20-storey building.

Wind loading controls some features of the design of building U20 only. For this building, the UBC wind design parameters are taken as follows: $I_w = 1$, wind speed = 113 kph, exposure B, $C_q = 0{\cdot}8$ for the windward side and 0·5 for the leeward side.

Analyses carried out in the design process use a planar-frame fibre model developed by the author. Capabilities of this computer program are summarized in the appendix. For the designs, composite slab action is neglected and the foundation is taken as rigid. The ultimate strength requirements for J6 and J20 are shown to be satisfied through push-over analyses which give ultimate strengths corresponding to base shear values of $0{\cdot}31W$ and $0{\cdot}13W$, respectively, which are adequate. The nominal yield strength of A36 steel is used in these calculations.

2.2. *Models for earthquake analysis*

The computer models used in the earthquake analysis of the four buildings are also half models and are made as realistic as possible so as to make the computed earthquake responses as realistic as possible. Frames B are present. Steel strengths are taken as 290 MPa (42·0 ksi) for yield and 345 MPa (50·0 ksi) for ultimate. Composite slab action and foundation interaction are included. Details appear in Reference 9; also refer to the appendix.

As in the static analysis, gravity loads are applied directly to the columns, and beams are not loaded within their spans. The same gravity loads are used in the dynamic analysis. For all buildings, masses for the horizontal and vertical frame degrees of freedom are based on these gravity loads (which include both dead and live parts) except that the floor live load for the horizontal-degree-of-freedom masses is reduced to 0·48 kPa (10 psf).

Viscous damping consists of a small amount (0·5 per cent) of stiffness-proportional damping at the fundamental mode plus a larger amount of inter-storey damping (see the appendix). The strength of the inter-storey dampers is taken to be equal to the storey shears produced by code seismic design forces which are based on a small fraction of the building seismic-design weight W: 0·02 for U6 and J6 and 0·01 for U20 and J20. The storey shear velocity at yield is set to 25 cm/sec for U6, 20 cm/sec for J6, and 10 cm/sec for U20 and J20 in order to give the same damping value of about 2·8 per cent (linear range of inter-storey dampers) for the fundamental mode of each building.

Two versions of each building are considered: one with all connections perfect and the other with fracture-prone connections present. Buildings with perfect (non-fracturing) connections are denoted by a suffix P, i.e. J6P. Buildings with fracture-prone connections are denoted by suffix F, i.e., U20F. Two sets of fracture strains for the welds (see the appendix) are defined:

Set F1, $\varepsilon_F = 10\varepsilon_Y$, $20\varepsilon_Y$, $40\varepsilon_Y$ and $80\varepsilon_Y$ at 30 per cent, 30 per cent, 20 per cent and 20 per cent, respectively;

Set F2, $\varepsilon_F = 0{\cdot}7\varepsilon_Y$, $2\varepsilon_Y$, $5\varepsilon_Y$, $15\varepsilon_Y$, and $40\varepsilon_Y$ at 20 per cent each, where each percent is a probability of occurrence. For the Case-F buildings, Set F2 is used for the bottom beam flange at the beam-to-column connections, and Set F1 is used for all other flange welds including beam-to-column, column splice and column base plate. The lower fracture strains for the bottom beam-flange welds reflect their poorer performance during the Northridge earthquake. The correspondence between strain in a flange weld and plastic hinge rotation for a lower-storey beam (no slab) in U6, J6, U20 and J20 is shown in Figure 2. From this figure, amounts of plastic rotation corresponding to fracture in the assumed model can be deduced.

The above percentages and fracture strains are intended to represent conditions in U.S. buildings built before the post-Northridge era of improved connections. Some correlation of the assumed fracture criteria to the Northridge earthquake experience using analyses of U6F and U20F is given in Section 2.5.

Computed first-mode elastic periods of the Case-P buildings without damping are

U6P,	1·54 sec
J6P,	1·16 sec
U20P,	3·47 sec
J20P,	3·04 sec

Geometric stiffness effects from gravity loads are included in the period calculation.

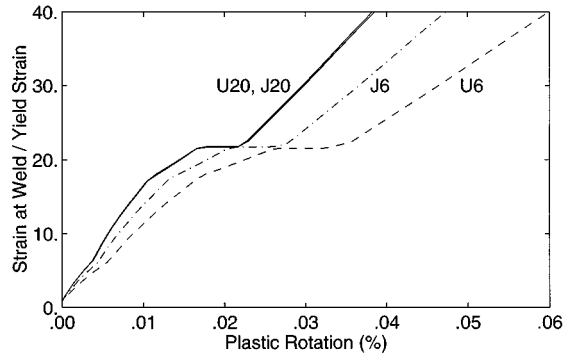

Figure 2. Axial strain in flange at end of girder (weld location) vs. plastic hinge rotation for lower-storey girders in the four buildings

2.3. *Push-over analyses*

To quantify the actual strength of each building, push-over analyses are run. In these analyses, the buildings are subjected to a slow, ramped, horizontal ground acceleration, and the building response is computed dynamically. The structural models are identical to those used in the earthquake analyses except that masses for the horizontal degrees of freedom are recalculated to total the seismic-design mass W/g with a distribution proportional to the seismic design loads. Thus, in this analysis technique, the lateral loads are essentially the horizontal seismic-design forces proportionally increasing with time at a slow rate. The base shear is computed by summing the horizontal components of the shear and axial forces in the first-storey columns, considering the updated geometries of these columns.

The push-over results show that the buildings are quite strong compared to the design base shears. Approximate ultimate lateral strengths (base shear) of each building as a fraction of its W value are computed to be

U6,	0·232 for U6P	0·187 for U6F
J6,	0·404 for J6P	0·314 for J6F
U20,	0·106 for U20P	0·083 for U20F
J20,	0·147 for J20P	0·114 for J20F.

These high strengths are a result of drift controlling the design in some cases and contributions from factors not considered in the design (composite slab action, inclusion of frames with simply connected beams, higher steel yield stress than the nominal value, and further increase in steel strength from strain-hardening). Inclusion of fracture-prone connections reduces a building's lateral strength; however, the residual strength is still well above the code-design base shear coefficients. For the Case-F buildings, three different random spatial distributions of the fracture strains are used in the push-over analyses, and the above values are the averages obtained.

2.4. *Connection fracture study*

In order to demonstrate the effects of connection fracture, a composite W30X116 beam which is connected to freely rotating W30X191 column stubs (Figure 3) is subjected at both ends to the rotation history shown in Figure 4. This substructure is taken from the 2nd-floor interior bay of Frame A of building U20 (see Figure 1), but the panel zones are set to be rigid. Beam-to-column connections are fracture prone at $\varepsilon_F/\varepsilon_Y = 10$ for the top flange welds and $\varepsilon_F/\varepsilon_Y = 0{\cdot}7$ for the bottom flange welds. Two situations are considered regarding axial restraint for the beam: complete restraint ($k = \infty$; see Figure 3) and no restraint ($k = 0$). The specified end rotations force the beam into double curvature as occurs under lateral loading from an earthquake.

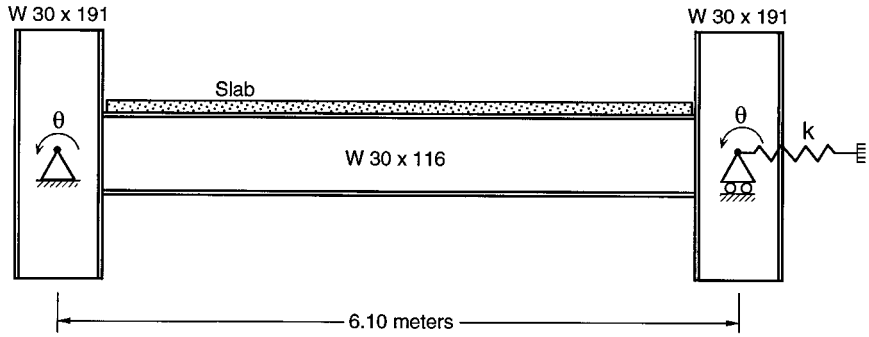

Figure 3. Set-up for connection fracture study. The spring stiffness k equals zero for no axial restraint, and k equals infinity for complete axial restraint

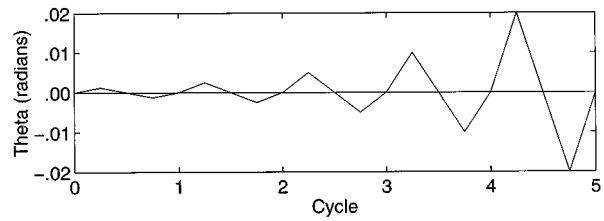

Figure 4. End rotation history of beam

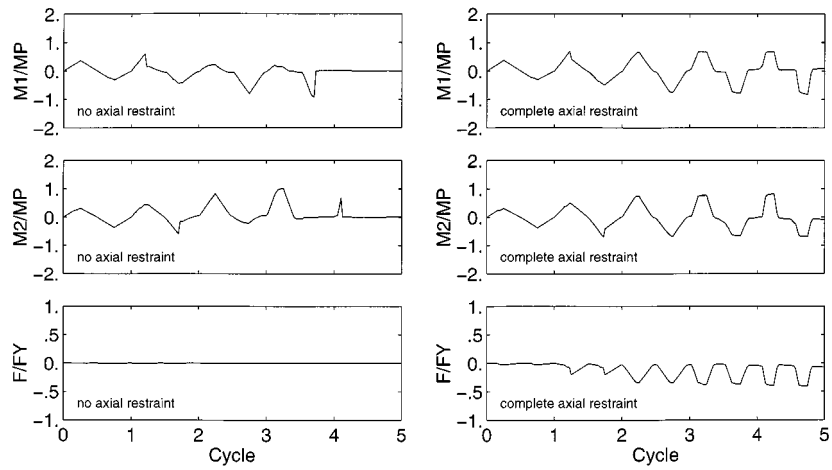

Figure 5. Results of bending beam example with fracturing connections

Results are presented in Figure 5 for moments M_1 and M_2 generated at the right and left ends of the composite beam and for the force F generated in the spring which provides the axial restraint. These quantities are plotted over the cyclic rotation history and are normalized with the plastic moment capacity M_P of the W beam section, in the case of M_1 and M_2, and with the axial yield force F_Y of the W beam section, in the case of F. M_P and F_Y are computed using the nominal yield stress. When axial restraint is not present, the moment capacity of the beam deteriorates to zero after a few cycles as the welds fracture. For complete axial restraint, a considerable amount of the moment capacity is retained. The amount of axial restraint for

beams in an actual building will be between the extremes considered in this example. The building models used in this paper contain some axial restraint which owes to frame action in the members connected to a beam, and so this restraint should be properly represented.

2.5. Northridge comparison

The fracture criteria given in Section 2.5 are consistent with the experience from the 1994 Northridge earthquake. To demonstrate this, buildings U6F and U20F are subjected to ground motions representative of those that struck a series of large steel moment frame buildings along the 101 freeway. This freeway runs east-west and passes 8 km south of the epicenter. Ground motions were recorded in basements of three of the buildings along an 11 km stretch of the freeway.[10] Since all three sets of ground motions are similar, any one of them can be taken as representative. The one used here is from site 2C246 which in the north–south direction has peak acceleration, velocity and displacement of 403 cm/sec^2, 56 cm/sec and 15 cm, respectively. This and the vertical component are employed in the analyses.

Results in terms of peak dynamic storey drift, residual roof displacement, and percentages of top and bottom beam-flange-to-column welds that fracture are summarized as follows.

	Peak dynamic storey drift	Residual roof displacement	Top flange fracture	Bottom flange fracture
U6F	2·3 %	7 cm north	10 %	36 %
U20F	0·6 %	< 1 cm	0 %	17 %

Each building was analysed 10 times using different random spatial distributions of fracture strains, and the above values are the averages obtained.

Many of the steel buildings along the 101 freeway had post-earthquake damage inspections, and a few details are repeated here for a 6-storey building[11] and a 17-storey one.[12] The 6-storey structure suffered significant damage to its two north–south moment frames. One of these had cracks in approximately 80 per cent of its beam-to-column connections, and the other had cracks in 40 per cent of these connections. Most of the fractures were at the bottom beam-flange weld, but some top flange welds were also cracked. Residual displacement at the roof was 7 cm to the north. Badly deformed anchors of the exterior precast concrete panels indicate that the dynamic storey drifts had been significant. The 17-storey structure had fractures to only its bottom beam-flange-to-column welds: 30 per cent to one north–south moment frame and 8 per cent to the other one. Residual displacement at the roof was about 15 cm to the north. Non-structural damage was less severe for this building than for the 6-storey one. Overall, the comparison between the behaviour of the analysed buildings and the real ones is favourable and gives some confidence to the fracture criteria employed in the analyses.

3. GROUND MOTIONS

Two sets of ground motions are employed in the earthquake analyses: motions from a simulation of the 1994 Northridge earthquake (M_W 6·7) produced by Dr David Wald of the USGS and motions from a simulated M_W 7·0 Elysian Park earthquake produced by Dr Wald and Prof. Thomas Heaton of Caltech. The simulated Northridge motions consist of both horizontal components and the vertical component. The simulated Elysian Park motions contain both horizontal components, but no vertical component. For use in the planar building analyses, the two horizontal components are resolved into the single horizontal component which maximizes the peak-to-peak ground velocity.

3.1. Northridge simulation

The first step in the simulation was to determine a source rupture model for the Northridge earthquake which is consistent with the available geodetic, leveling, strong motion, and teleseismic data. This work is

described in Reference 13. Next, a square grid of target sites was chosen in the near-fault area, in this case 144 sites over an area of approximately 3600 km^2 at a station spacing of about 5 km. Using the source model, long-period ground motions (> 1 sec period) were computed for each grid station. The grid of stations used is shown in Fig. 6 as small circles; open circles depict rock sites and solid circles represent soil sites. Green's functions at rock and soil sites were computed with different velocity structures to better approximate the shallow impedance contrasts.

For each grid station, high frequency (< 1 sec period) ground motions were taken from an actual earthquake recording made nearby so as to best approximate the correct directivity, site conditions, and epicentral distance. Locations of the actual recordings are shown as triangles in Figure 6, and each of these locations together with its associated group of grid stations are enclosed by a solid line. A matched pair of filters was used to remove the short periods from the computed records and to remove the long periods from the actual records, and then the pairs of filtered records were summed to produce the final ground motions.

A subset of the 144 grid sites consisting of the inner 10×10 grid is used in this study. For the horizontal component, the largest acceleration is 854 cm/sec^2 at site H06; the largest velocity is 176 cm/sec at site H04; and the largest displacement is 61 cm at site H06. Time histories and the pseudo-acceleration response spectrum (5 per cent damping) for site H04 are presented in Figure 7. For reference, in the pseudo-acceleration plot, the first-mode periods of the Case-P buildings are marked.

The ground motions produced in the simulation which are most damaging to the buildings considered here contain strong near-source effects, but they also occur at soil sites where some amplification of the motion takes place. Rupture on the fault starts at the epicenter, located below and between grid sites C07 and

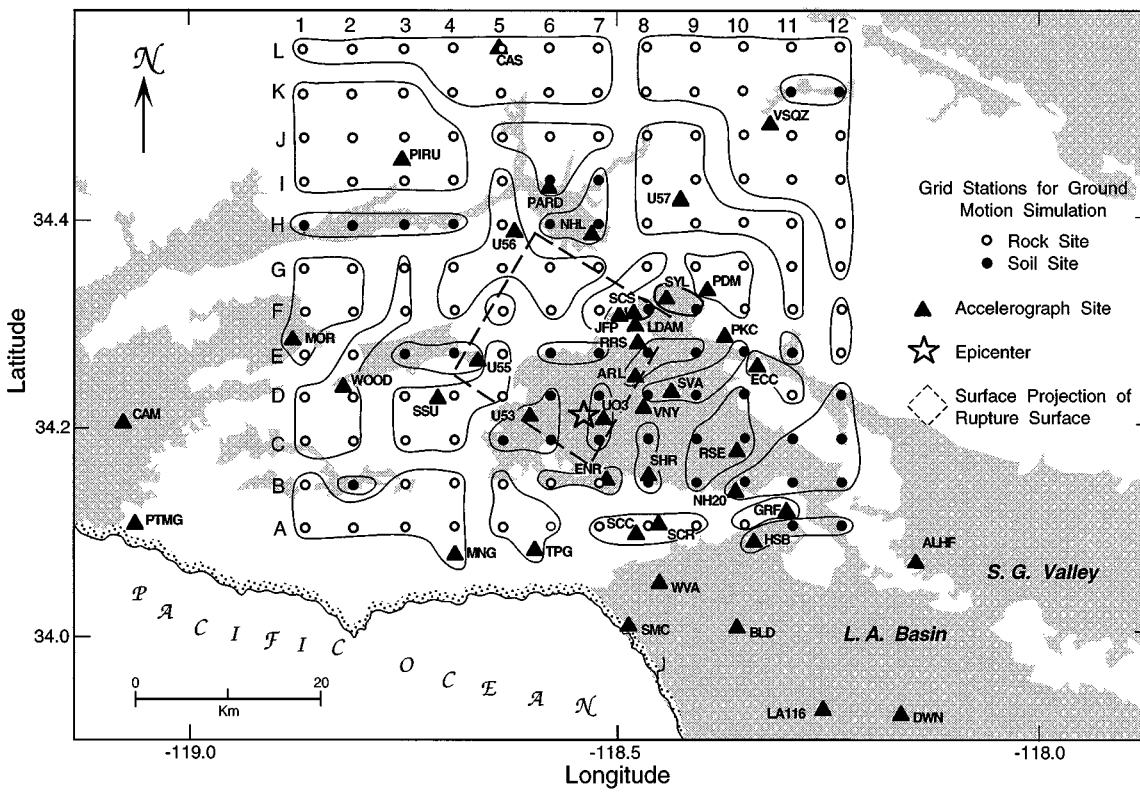

Figure 6. Map of San Fernando Valley and vicinity showing 144 grid stations for the ground motion simulation for the Northridge earthquake. The shaded zones are basin areas

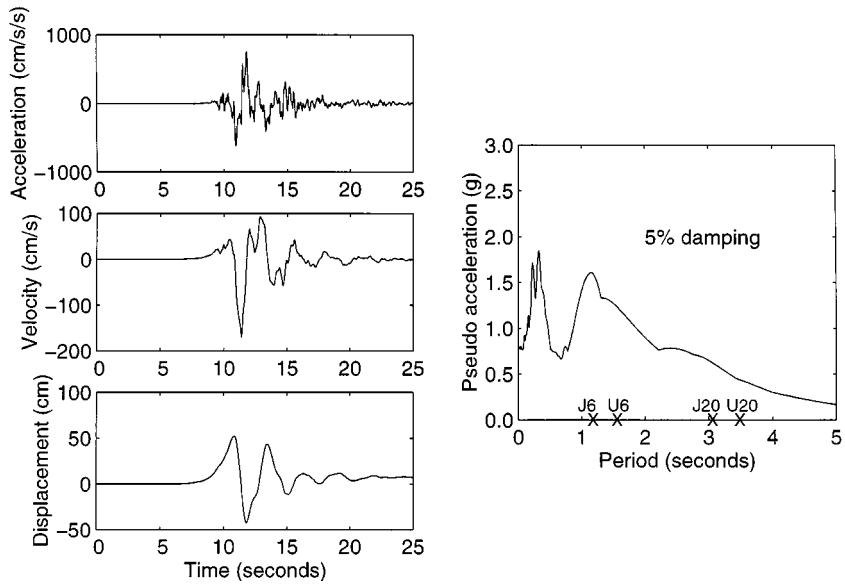

Figure 7. H04 horizontal ground motion time history and pseudo-acceleration spectrum from the simulated Northridge earthquake

D07, and propagates to the north within the sector between northeast and northwest. The region in this direction where the extended fault plane intersects the ground surface is where the strong near-source effects are found. Few sizable buildings were actually located in this area.

3.2. Elysian Park simulation

This hypothetical event is consistent with a possible M_W 7·0 earthquake on the Elysian Park blind-thrust fault directly beneath Los Angeles. Geometry of the simulation is shown in Figure 8. The fault dips 23° to the north in a vertically stratified crustal model which approximates the rock properties in the Los Angeles Basin. The rupture surface is 35 km long and 18 km wide and is confined to depths between 9 and 16 km.

As details of the simulation are discussed in Reference 6, only a short summary is included here. The procedure is similar to that used for the Northridge earthquake in that the long periods (>1 sec) are computed deterministically by a Green's function approach and the short periods are taken from actual recordings. The fault slip historey is that determined previously for the Homestead Valley segment of the 1992 Landers earthquake adjusted to fit the characteristics of the subject earthquake. Resulting average and peak slips for the simulation are 2·2 and 5·1 m, respectively, and the direction of the rupture propagation is up-fault. The actual recordings supplying the short periods are from the 1994 Northridge earthquake; the free-field record at the Olive View Hospital is used for sites in the direction of the rupture propagation, and the Stone Canyon Reservoir record is used elsewhere.

Ground motions are simulated on the rectangular grid of sites in Figure 8, 11 stations $\times$ 11 stations at a 5 km grid spacing covering 3025 km^2. The largest acceleration is 1040 cm/sec^2 at site I05; the largest velocity is 180 cm/sec at site H05; and the largest displacement is 200 cm at site D05. The area which experiences a peak displacement over 1 m is about 600 km^2 in extent, and over most of this area the peak velocity exceeds 1 m/sec. Time histories and the pseudo-acceleration response spectrum (5 per cent damping) for site H05 are presented in Figure 9.

Similar to what is shown in Figure 9, ground motions at many of the sites toward which the rupture propagates are dominated by a large forward-and-back displacement pulse, this being the near-source effect. This displacement reaches an amplitude of 2 m at site D05 and is much greater than any ground

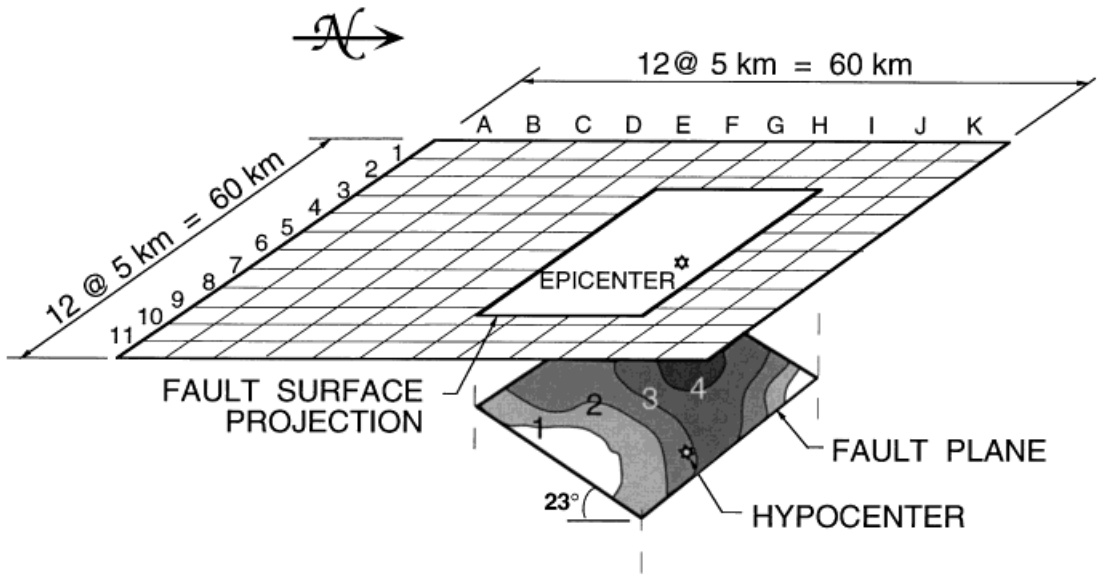

Figure 8. Details of the M_W 7·0 Elysian Park earthquake simulation showing the dipping fault plane, contours of fault slip in meters, and 121 grid stations where motions are computed

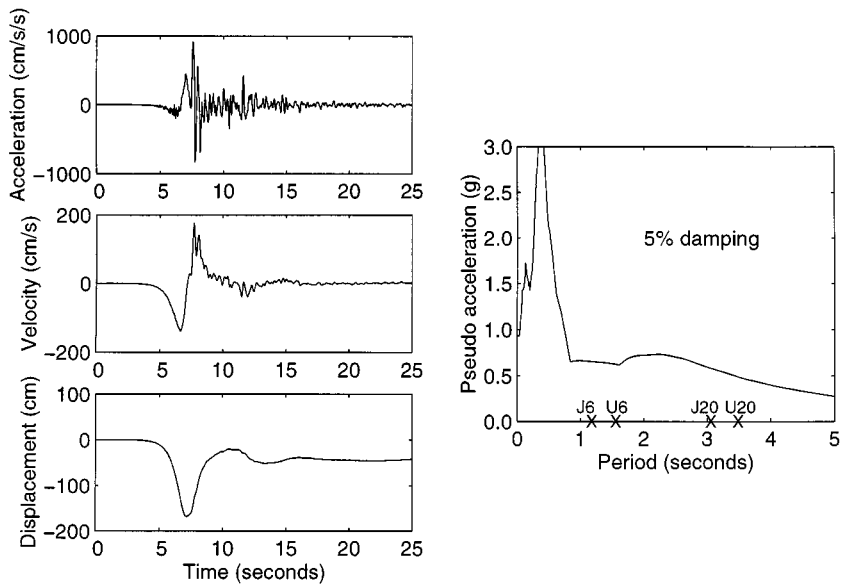

Figure 9. H05 horizontal ground motion time-history and pseudo-acceleration spectrum from the simulated Elysian Park earthquake

displacement associated with the Northridge earthquake. The size of this displacement owes to the larger magnitude of the hypothetical Elysian Park event.

4. RESULTS

All four buildings are analysed for the ground motions described in the previous section. Connections are considered to be either non-fracturing (Case P) or fracture-prone (Case F). For Case F, a different random

spatial distribution of fracture strains is used for each site in the Northridge and Elysian Park simulations. Additional results appear in Reference 9.

4.1. Northridge simulation

Results for the simulated Northridge ground motions are obtained on the inner 10×10 grid of sites. A comparison of the peak ground motion parameters over the region with the computed responses shows that building damage (as quantified by the number of weld breaks and maximum drift) correlates best to peak ground displacement and velocity. One of the most damaging ground motions is at site H04 where the peak horizontal ground displacement and velocity are 52 cm and 176 cm/sec (Figure 7). At this site the peak storey drift can reach large values, for example, 7·6 per cent for building U6F. Although the computer program does not show collapse at site H04 for building U6F, the large drift is in a range where deterioration mechanisms not included in the computer program, such as local flange buckling, play an important role, and so collapse should not be ruled out.

The study shows that the percentage of welds which fracture is often quite high for the beam flanges. At site H04 for building U6F, where the 7·6 per cent storey drift occurs, 33 per cent of the top beam-flange-to-column welds fracture as do 69 per cent of the bottom ones. Even when the response is much less, often a considerable number of connections still fracture. For building J6F at site C06, 7 per cent of the top beam-flange welds and 41 per cent of the bottom ones fracture, and the maximum storey drift is only 1·7 per cent. Stability of a building in the presence of a high percentage of fractured connections is due to the welds which do not fracture as well as the residual strength remaining in the fractured connections. This residual strength as modelled by the program can be significant, especially with composite slab action and some axial restraint to beams present.

A summary of the storey drifts appears in Figure 10 for the 6-storey buildings and in Figure 11 for the 20-storey buildings. Plotted are the number of sites where peak storey drift exceeds 2 per cent, the data being

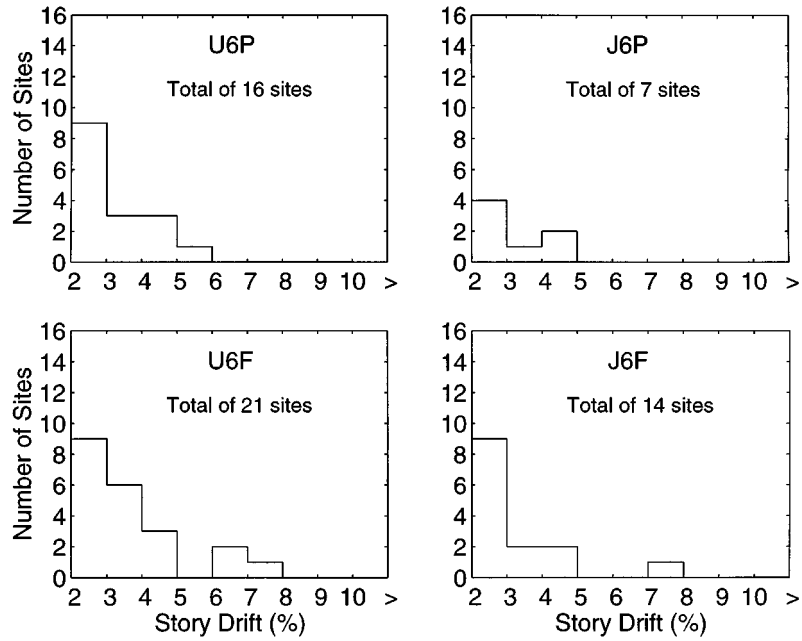

Figure 10. Summary of maximum storey drifts for the 6-storey buildings to the simulated Northridge earthquake. Each site represents an area of 5 km × 5 km

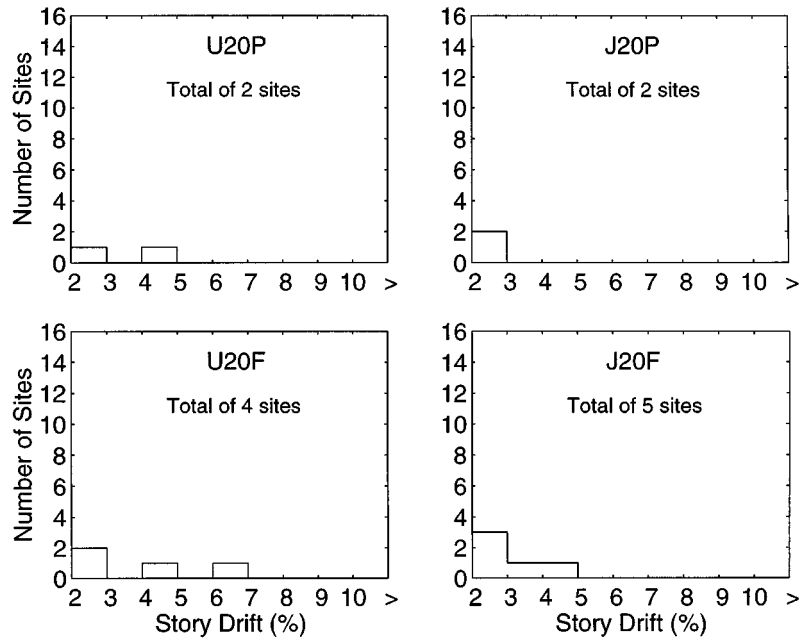

Figure 11. Summary of maximum storey drifts for the 20-storey buildings to the simulated Northridge earthquake. Each site represents an area of 5 km × 5 km

for 1 per cent increments of drift. Each site represents 25 km^2. From these plots, general conclusions can readily be made about the role of building height, the benefits of higher lateral strength, and the effects of connection fracture. Regarding building height, storey drifts are much greater for the 6-storey buildings than the 20-storey buildings. The pseudo-acceleration response spectrum in Figure 7 shows larger ordinates for the shorter buildings, consistent with their greater drifts. These larger drifts occur despite the shorter buildings being much stronger than the taller ones relative to their own weights.

Some benefits are gained by increasing a building's lateral strength, as seen from Figures 10 and 11 by comparing the Japanese designs to the UBC ones, but they are modest. This probably has to do with the accompanying increase in stiffness attracting more load. As also seen from Figures 10 and 11, connection fracture according to the Case-F assumption has a detrimental effect, but it is not catastrophic. Helpful here are the post-fracture residual strength in the connections and the fact that, in the analyses, a significant number of connections are assigned fracture strains high enough so that fracture does not occur.

The trends evident from Figures 10 and 11 are averages. Individual cases occur where increasing the lateral strength causes a larger response and where permitting connections to fracture reduces the response. The results are influenced by many factors such as frequency content of the earthquake, a building's vibrational frequencies, and non-linear effects.

4.2. Elysian Park simulation

Results for the Elysian Park motions are obtained at all sites of the 11 × 11 grid. Summaries of the storey drifts above 2 per cent appear in Figure 12 for the 6-storey buildings and in Figure 13 for the 20-storey buildings. Each site represents 25 km^2.

The level of response for the Elysian Park earthquake significantly exceeds that for the Northridge earthquake because of the much larger ground displacement which occurs in the M_W 7·0 Elysian Park event. This is especially true for the 20-storey buildings for which the long forward-and-back displacement pulse which dominates the motion is a very effective excitation. For Case F, both the UBC and Japanese-designed

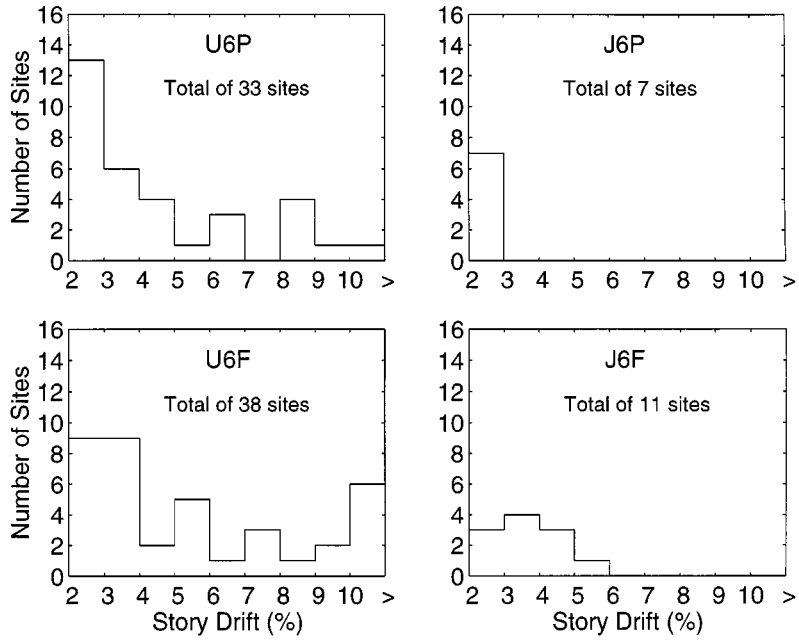

Figure 12. Summary of maximum storey drifts for the 6-storey buildings to the simulated Elysian Park earthquake. Each site represents an area of 5 km × 5 km

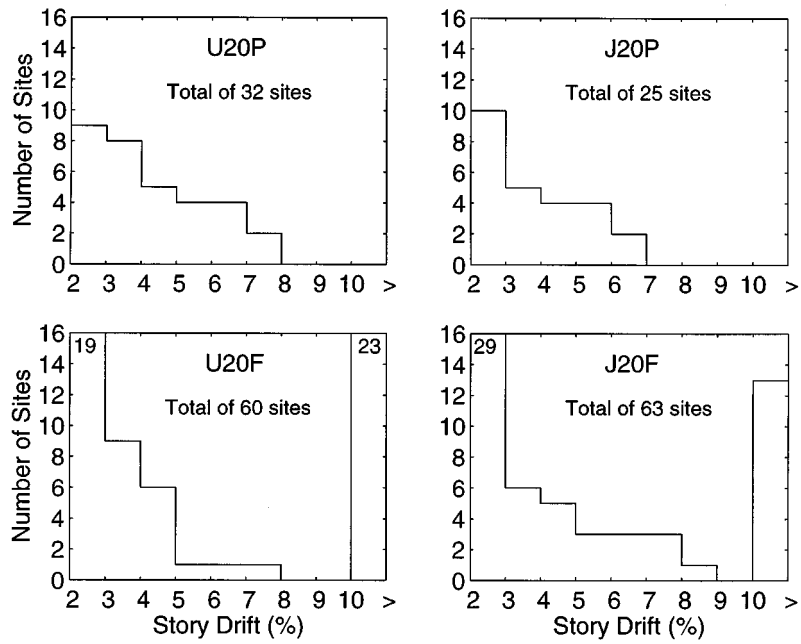

Figure 13. Summary of maximum storey drifts for the 20-storey buildings to the simulated Elysian Park earthquake. Each site represents an area of 5 km × 5 km

20-storey buildings experience 2 per cent or significantly greater drift at sites representing a huge area of about 1500 km^2, with large drifts occurring over a third or more of this area. Regarding the 6-storey building, the UBC design is also hit hard by the Elysian Park earthquake, but the Japanese design, owing to its higher strength, shows a much improved behaviour. For all of the buildings, connection fracture has a significantly detrimental effect for the Elysian Park earthquake, more than what was seen for the smaller Northridge event. Most of the fractures occur in the beam-to-column connections; column-splice fracture plays only a minor role in these results.

5. CONCLUSIONS

U.S.-designed buildings have considerably greater strength than indicated by the code lateral force coefficient V/W. For the 6-storey building U6P (P: perfect connections) designed according to the 1994 UBC, $V = 0{\cdot}044W$, but the push-over analysis shows an ultimate lateral strength of 0·232W (with perfect connections). For the 20-storey UBC-designed building U20P, the values are $V = 0{\cdot}03W$ (code) and $0{\cdot}106W$ (push-over with perfect connections). The extra strength is due to the drift requirements in the code, the code's safety factor, and the contributions from higher-than-nominal steel strength, strain hardening, composite slab action, and the gravity frames.

The strongest of the ground motions from the simulated M_W 6·7 Northridge earthquake hits the 6-storey buildings hard, not only the UBC-designed U6P, but the stronger J6P. The push-over strength of J6P is $0{\cdot}404W$, and this increase in strength has benefit in reducing storey drift. For example, for the Northridge earthquake simulation, building U6P experiences storey drifts of 2 per cent or greater at 16 sites (25 km^2 per site) with a peak drift of 5·0 per cent, and the stronger J6P experiences such drift at 7 sites with a peak drift of 4·5 per cent. The 20-storey buildings are hit less hard. For the Northridge simulation, both U20P and J20P (push-over strength of 0·147W) experience drifts of 2 per cent or greater at only 2 sites.

The M_W 7·0 Elysian Park earthquake, with its large displacement pulse, severely affects the UBC-designed buildings, both the 6-storey and 20-storey ones. Drifts of 2 per cent or greater occur at 33 sites for U6P and at 32 sites for U20P. Maximum drifts are 10·5 per cent and 7·8 per cent, respectively. Strengthening is beneficial for the Elysian Park earthquake, especially for the 6-storey building. J6P experiences storey drifts of 2 per cent or greater at only 7 sites (maximum of 2·9 per cent); however, J20P still experiences such drifts at 25 sites (maximum of 6·5 per cent). The 25 sites for J20P represent an area of 625 km^2, a large area for a strengthened design to receive significant damage in a M_W 7·0 earthquake.

Connection fracture is detrimental because it increases storey drifts and the possibility of collapse. The model for connection fracture employed here which uses the Case-F assumptions reduces the push-over strengths by about 20 per cent; even so, the residual strength is still well above the code design-force level. For the Northridge earthquake simulation, storey drifts of 2 per cent or greater are experienced by U6F, J6F, U20F and J20F at 21, 14, 4, and 5 sites, respectively, compared to 16, 7, 2 and 2 sites, respectively, with perfect connections. Storey drifts in the Case-F buildings above 6 per cent, for which collapse cannot be ruled out, occur at a few sites. For the Elysian Park simulation, U6F, J6F, U20F and J20F experience storey drifts of 2 per cent or greater at 38, 11, 60 and 63 sites, respectively, compared to 33, 7, 32 and 25 sites, respectively, with perfect connections. Many of these sites show either large storey drifts or collapse for the Case-F buildings. For example, for U20F there are 25 sites with storey drifts at or above 6 per cent, and at 22 of these the computer program actually predicts collapse. The 22 sites represent a large area of 550 km^2. Assuming the present modelling scheme is valid, these results indicate that the connection fracture problem in existing buildings significantly increases the risk of collapse in large earthquakes.

In summary, this investigation has quantified near-source effects on buildings during moderate earthquakes such as Northridge and during a larger M_W 7·0 earthquake. These earthquakes are capable of causing significant wide-spread damage to existing steel buildings in the U.S., including collapse, especially for the larger earthquake and if the connections in the buildings are fracture-prone. The most severe ground motions from such earthquakes present a challenge to designers who want to limit storey drifts to 2 per cent. Stouter

connections and stronger buildings are beneficial, but the accompanying increase in stiffness can attract more load and offset some of the expected gain in performance. However, the best design philosophy for large earthquakes such as the M_W 7·0 event considered here does appear to be strong, short buildings. The economics of improved designs can be evaluated by weighing the extra construction costs with the estimates of damage from studies like the present one.

If the large increment in damage and collapse potential from a M_W 6·7 to a M_W 7·0 earthquake, as demonstrated here, is not intuitive, perhaps it is because of the lack of actual experience with a large earthquake directly striking a major city. Or, perhaps the ground motions from the simulated Elysian Park earthquake have been overestimated. Realistic simulation of ground motion from large earthquakes is a critical area which needs to develop further. Other future work which verifies and extends the present study is needed to:

(a) improve the structural models, especially with regards to nonstructural contributions to strength and stiffness, structural degradation mechanisms including weld fracture, and foundation interaction;
(b) examine buildings of other heights and types, including very tall buildings;
(c) incorporate three-dimensional structural modelling capabilities to capture torsion and effects of building irregularity;
(d) examine effects of soft soils;
(e) quantify the effects of even greater earthquakes which have not only large ground displacements but long durations of shaking.

Reported in Reference 9 are additional results for a simulation of the M_W 6·9 Kobe earthquake and other results for buildings whose connections are more fracture prone than the Case-F buildings considered here.

6. POSTSCRIPT

The 1996 SEAOC *Blue Book*[14] contains proposed near-source factors which increase the design base shear for sites close to active faults. These factors depend on the type of source (A, B or C) and the distance from the fault ($\leqslant 2$ to 15 km). Source A must be capable of generating a $M_W \geqslant 7$ earthquake and have a slip rate $\geqslant 5$ mm/y. The Source C earthquake has $M_W < 6{\cdot}5$ and a slip rate $\leqslant 2$ mm/y. Intermediate sources are classified as B. For thrust faults like the ones considered in this paper, the fault distance is measured from the surface projection of the part of the fault which is within 10 km of the surface.

Each of the four buildings U6, J6, U20 and J20 (design models of Section 2.1) is evaluated according to the static lateral force procedure of the proposed code provisions. First, lateral loads are applied until either the allowable stresses or allowable drifts are exceeded, and these loads are expressed in terms of V/W for each building (W being dead weight only). Then, design values of V/W are computed by the code formulas using source and fault distance combinations which produce values of the near-source factor N_v of 1·2 (A at 10 km or B at 5 km), 1·6 (A at 5 km or B at $\leqslant 2$ km) and 2·0 (A at $\leqslant 2$ km). Accidental eccentricity and reductions in applied load used in the drift calculation are taken into account. Also: Zone 4, $R = 3.4 \cdot 2{\cdot}5$, soil S_D, $I = 1$, and $T = 0{\cdot}035 \cdot (h_n)^{0{\cdot}75}$ times 1·4 for U6 and U20 or 1·3 for J6 and J20.

Comparison of the two V/W values for each building yields the margin by which each building exceeds or falls short of the new provisions. These margins are summarized in the following.

	$N_v = 1{\cdot}2$	$N_v = 1{\cdot}6$	$N_v = 2{\cdot}0$
U6	− 20 %	− 40 %	− 52 %
J6	+ 73 %	+ 30 %	+ 4 %
U20	+ 30 %	− 2 %	− 22 %
J20	+ 78 %	+ 33 %	+ 7 %

Both of the Japanese-designed buildings exceed the most stringent near-source requirement ($N_v = 2{\cdot}0$). While neither U6 nor U20, both designed under the 1994 UBC, would be expected to satisfy any of these

requirements, U20 does in fact exceed the $N_v = 1{\cdot}2$ level and nearly meets the $N_v = 1{\cdot}6$ level. Recall that for the UBC designs, the allowed reduction in load used in the drift calculation was not taken, and this imparts significant conservatism to U20.

Provisions of the 1997 Uniform Building Code are similar to the 1996 SEAOC ones with the exception that SEAOC base shear equation 45–76 can not be disregarded in the drift computation. This makes a big difference for tall buildings, and the above margins for U20 and J20 change as follows:

	$N_v = 1{\cdot}2$	$N_v = 1{\cdot}6$	$N_v = 2{\cdot}0$
U20	− 17 %	− 38 %	− 50 %
J20	+ 22 %	− 8 %	− 27 %

The above information allows the results in this paper to be interpreted relative to the proposed near-source provisions contained in the 1996 SEAOC *Blue Book*. For this purpose, the Northridge earthquake could be considered as Source B and the Elysian Park earthquake as Source A. It should be noted that, for both of these blind-thrust earthquakes, many of the sites where damage is predicted lie beyond a 5 km fault distance as defined.

APPENDIX

I.1. Computer program

Computations in this study were carried out with a planar frame analysis computer program based on the fibre method and written especially for steel structures. Details of the formulation can be found in references 9, 15 and 16.

I.2. Planar frame model

A frame consists of a planar arrangement of beams, columns and panel zones (Figure 14), all of which can exhibit nonlinear behavior. The panel zones occupy the joint regions and to them are connected the beams (at the sides) and the columns (top and bottom). Each panel zone is a rectangular element which deforms in shear, and its actual dimensions are represented. The shear strain in the panel zone is the difference between the end rotation of the connected beams and the end rotation of the connected columns. Two connected beams have the same end rotation as do two connected columns. Beam and column members are modelled by the fibre method wherein each member is subdivided along its length into segments (Figures 14 and 15) and within its cross-section into fibres (Figure 15).

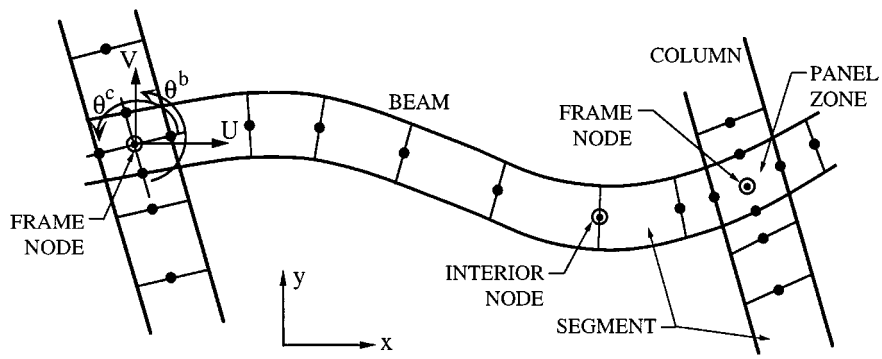

Figure 14. Details of planar frame model

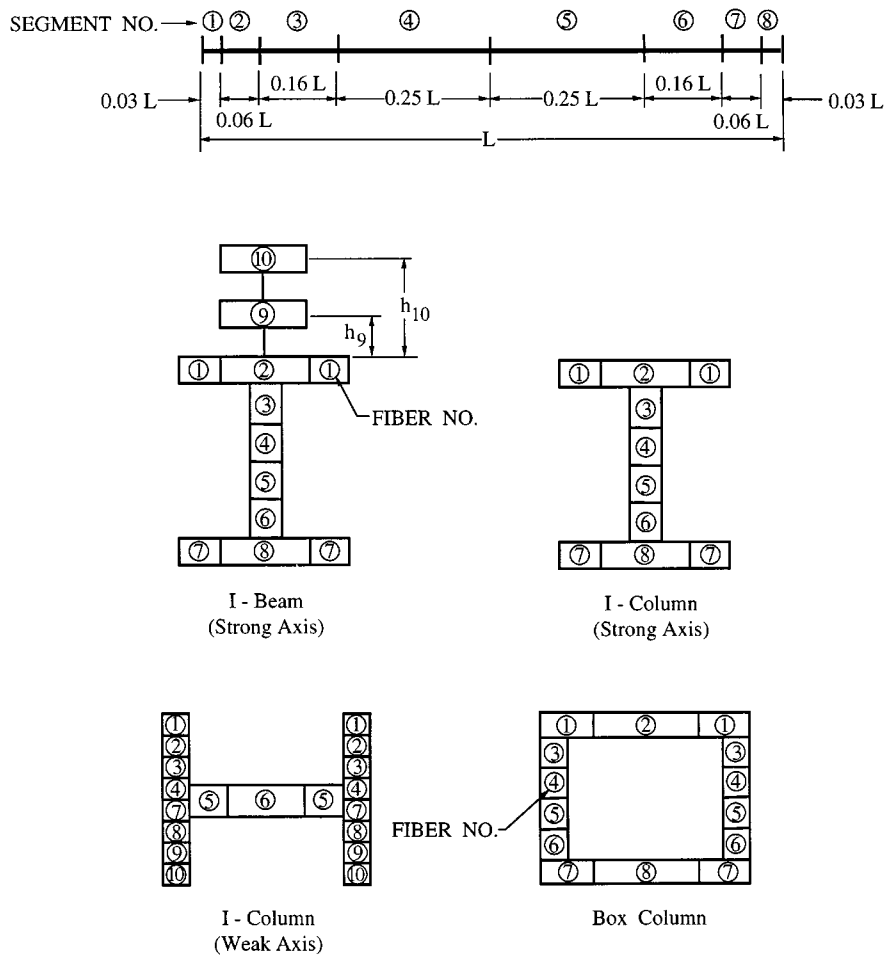

Figure 15. Segment layout (top) and fibre layout (bottom) for beams and columns

There are four degrees of freedom at each joint in the frame model: horizontal and vertical translations plus the beam-ends and column-ends rotations. Mass is lumped into the translational degrees of freedom. Interior degrees of freedom in the beam and column members are massless, and this allows them to be dealt with locally and left out of the frame matrices.

I.3. Panel zone

The load on a panel zone is a double couple derived from the end moments and shears of the connected beams and columns, one couple coming from the beam end moments and column shears and the other coming from the column end moments and beam shears. Behavior of a panel zone is defined by a non-linear hysteretic relation between this moment and the resulting shear strain. No degradation in strength is included in the hysteretic model.

A capability exists to account for the addition of doubler plates by increasing the thickness of the panel zone. Without doubler plates, the panel zone thickness is the same as the column web thickness.

I.4. Beam and column elements

These elements are divided into segments along their length and into fibres within their cross-section (Figure 15). Columns can be oriented either by their strong or weak axis. Eight segments and ten fibres are used as shown in Figure 15. Fibres 9 and 10 in the strong-axis orientation are used only for a beam to represent composite action with a metal deck and concrete slab.

Associated with each segment is a linear shear stiffness and associated with each fibre is an axial stress–strain relation. The shear stiffness is based on the cross-sectional area of the steel plates which are in the plane of the frame. The stress–strain relation for fibres 1–9 is that of a steel bar subjected to axial stress and is non-linear and hysteretic with strain hardening and residual stresses included. Connection fracture (Section I.5) is the only strength degradation mechanism. The stress-strain behaviour of the concrete fibre is linearly elastic–perfectly plastic in compression and linear to cracking in tension. Cracking releases the tensile stress and no tension can be subsequently carried. Once formed, a crack can later close and carry compression.

A simple connection (non-moment-resisting) is modelled by reducing the areas of the fibres in the two adjacent segments at the end of the beam where the connection is located — either segments 1 and 2 or segments 7 and 8 or both pairs. The areas of the flange fibres 1, 2, 7 and 8 are zeroed, and the areas of the web fibres 3–6 are reduced by an amount appropriate to represent the flexibility of a bolted web plate. The web fibre area reduction may also be appropriate for moment connections.

I.5. Weld fracture

Steel fibres in the end segments 1 or 8 of a beam are given the capability to fracture when the strain reaches some specified value. A fractured fibre releases its tensile stress and loses its ability to carry tension in the future, but it can carry compression if contact is later regained. For a column (segment 1 is at the bottom; segment 8 is at the top), the fibre fracture capability is used for splice welds and for welds to base plates. Column segment 4 is used for the splice weld and segment 1 for the base-plate weld.

A fracture strain ε_F is assigned to a fibre using a randomized process. Sets of fracture strains are established with associated probabilities of occurrence in units of 10 per cent. An example of a set is: $\varepsilon_F = 0{\cdot}7 \cdot \varepsilon_Y$ at 20 per cent; $\varepsilon_F = 1{\cdot}0 \cdot \varepsilon_Y$ at 50 per cent; $\varepsilon_F = 2{\cdot}0 \cdot \varepsilon_Y$ at 30 per cent, where ε_Y = yield strain. Fibres to be assigned fracture strains are placed into groups of which there are four types: column splice, column base plate, top beam flange and bottom beam flange. A group of column-splice fibres consists of all eight fibres of segment 4 in a column containing a splice. A group of column-base-plate fibres consists of all eight fibres of segment 1 in a column attached to a base plate. A group of top beam-flange fibres consists of fibres 1 to 4 in segment 1 or 8 where a moment connection exists, similar for a bottom beam-flange group except that the fibres are 5–8. Each group type is associated with one of the sets of fracture strains. Once the sets of fracture strains and the groups of fibres are established, the fracture strains are assigned randomly to the groups within each type using the specified occurrence probabilities of the associated set. All fibres in a group receive the same fracture strain, but the fracture strain would vary from group to group within each type throughout the building.

If all fibres of a column splice fracture, the column is assumed not to carry any load thereafter. The assumption here is that the lateral offset of the storey would be sufficient to bring the column-section plates out of alignment, and so the load-carrying capacity would be reduced dramatically. If all beam fibres of a beam-to-column connection fracture, the shear transfer capacity is assumed to remain intact. In addition, for a beam or a partially cracked column splice, compressive fibre stresses can be transferred through parts of the cross-section which later reestablish contact. The column-to-base-plate connection is handled similarly to the beam-to-column connection.

I.6. Wall and foundation elements

Each basement storey bay can be constrained against lateral motion by a wall element which connects the top and bottom joint nodes of two adjacent columns. The wall element resists shear deformation and does

not oppose rigid-body rotations. In addition, some axial stiffness is provided to the beam and column members of the frame on the perimeter of the wall element. All of these features are linearly elastic.

Foundation interaction is included through a horizontal and vertical spring attached to the bottom of each column line. Each spring is bilinear, and the hardening behaviour is kinematic.

I.7. Solution technique

In the analysis, gravity loads are applied first followed by the earthquake loading. Ground motions can have both a horizontal and a vertical component present. The equations of motion involving the frame joint degrees of freedom are integrated implicitly with iterations in each time step until convergence is achieved. The tangent stiffness matrix is used in this process. The matrix solution in each iteration produces increments in the displacements of the four degrees of freedom at each frame joint. From these, the increments in the end displacements of each beam and column are computed and applied to these members. Each beam and column is then solved individually for its end forces and shears which are fed back to the frame equations and assembled into the right-side residual vector. The individual beam and column solutions also provide contributions to the frame tangent stiffness matrix. Because the beams and columns exhibit non-linear behavior, their individual solutions are iterative as well. Contributions to the right-side residual vector and the tangent stiffness matrix in the frame iterations also come from the panel zones, foundations springs and basement walls.

Damping is handled in a non-standard way to avoid the large damping forces that can occur in a non-linear analysis when the damping matrix contains a term proportional to the linear stiffness matrix. Although use of linear damping is common in non-linear analyses, the viscous forces generated can be on the order of the forces carried by the structural frame, which is both unrealistic and unconservative. Such damping forces occur after yielding of the frame when the velocity of storey drift reaches a high value. In the present formulation, damping is provided as capped viscous dampers placed alongside each column so as to oppose the relative floor-to-floor horizontal velocity. The capping is on the force carried by these inter-storey dampers. The cap values can be set so that the capacity of all dampers in a storey equals the shear force for that storey produced by code seismic design forces which are based on a fraction (say, 0·01 or 0·02) of the building seismic-design weight. The damper 'stiffness' can be set by specifying the storey drift velocity at which the cap is reached. Some additional but very small amount of linear stiffness-proportional damping is used for numerical purposes.

During the response, the co-ordinates of the frame joints are updated, and in this way P-delta effects due to gravity loads carried by all the included frames are accounted for. If there are other frames in the building which carry gravity loads but are not included in the analysis, their contributions to P-delta effects can be incorporated through storey shear forces which are applied to the included frames.

Coordinate updating is also applied to the connectivity of the beams, columns and panel zones and to the interior nodes of the beams and columns. The latter means that moment amplification and member buckling (but not local flange buckling) are accounted for. For brace members, this procedure gives a good representation of buckling and post-buckling behaviour under cyclic loads.

A building consisting of several parallel frames can be analysed for loads in the plane of these frames by including the various frames in the model. Each frame is defined independently and then they are hooked together by constraint matrices. An individual constraint matrix connects the horizontal joint degrees of freedom on one floor of one frame to those on the same floor of another frame, and the condition imposed is that the average displacement of the first set of degrees of freedom equals the average for the second set of degrees of freedom. The idea of using the average displacement is to allow for the length changes in the beams which occur under cyclic loading and especially after weld fracture. If some of the parallel frames are identical, they can be lumped into a single frame by specifying an equivalent width multiplier.

ACKNOWLEDGEMENTS

This research was partially supported by the Kajima-CUREe Joint Research Program, Phase II: mitigation of the effects of earthquakes and other natural hazards for safety of urban areas.

REFERENCES

1. International Conference of Building Officials, *Uniform Building Code*, Whittier CA, May 1994.
2. International Association of Earthquake Engineering, 'Earthquake resistant design method for buildings', *Earthquake Resistant Regulations A World List—1992*, Chapter 23, Part 2, Tokyo Japan, July 1992, pp. 23–55 to 23–71.
3. J. C. Anderson and V. V. Bertero, 'Uncertainties in establishing design earthquakes', *J. Struct. Engng. ASCE*, **113**, 1709–1724 (1987).
4. V. V. Bertero, S. A. Mahin and R. A. Herrera, 'Aseismic design implications of near-fault San Fernando earthquake records', *Int. J. Earthquake Engng. Struct. Dyn.* **6**, 31–42 (1978).
5. C. W. Roeder, S. P. Schneider and J. E. Carpenter, 'Seismic behavior of moment-resisting steel frames: analytical study', *J. Struct. Engng.* **119**, 1866–1884 (1993).
6. J. F. Hall, T. H. Heaton, M. W. Halling and D. J. Wald, 'Near-source ground motion and its effects on flexible buildings', *Earthquake Spectra EERI* **11** (1995).
7. J. F. Hall, 'Parameter study of the response of moment-resisting steel frame buildings to near-source ground motions', *Report No. EERL 95-08*, Earthquake Engineering Research Laboratory, Caltech, Pasadena CA, December 1995.
8. B. F. Maison and K. Kasai, 'Analysis of Northridge Damaged Thirteen-Story WSMF Building', *Earthquake Spectra EERI* **13** (1997).
9. J. F. Hall, 'Seismic response of steel frame buildings to near-source ground motions', *Report No. EERL 97-05*, Earthquake Engineering Research Laboratory, Caltech, Pasadena, CA, June 1997.
10. California Division of Mines and Geology, 'Los Angeles code-instrumented building records from the Northridge, California earthquake of January 17 1994; processed release No. 1', *Report No. OSMS 94-17*, 30 December 1994.
11. V. V. Bertero, J. C. Anderson and H. Krawinkler, 'Performance of Steel Building Structures During the Northridge Earthquake', *Report No. UBC/EERC-94/09*, Earthquake Engineering Research Center, University of California, Berkeley, August 1994.
12. T. F. Paret and K. K. Sasaki, 'Analysis of a 17-Storey Steel Moment Frame Building Damaged by the Northridge Earthquake', *Technical Report*: *Analytical and Field Investigations of Buildings Affected by the Northridge Earthquake of January 17, 1994*, Chapter 10, SAC 95-04, Part 2, December 1995.
13. D. J. Wald, T. H. Heaton and K. W. Hudnut, 'The slip history of the 1994 Northridge, California, earthquake determined from strong-motion, teleseismic, GPS, and leveling data', *Bull. Seism. Soc. of Amer.* **86**, S49–S70 (1996).
14. Structural Engineers Association of California, *Recommended Lateral Force Requirements and Commentary*, Appendix C—SEAOC Strength Design Code Change Proposal, October 1996.
15. M. Challa and J. F. Hall, 'Earthquake collapse analysis of steel frames', *Earthquake Engng. Struct. Dyn.* **23**, 1199–1218 (1994).
16. J. F. Hall and M. Challa, 'Beam-column modeling', *J. Engng. Mech. ASCE* **121** (1995).

